JOURNAL OF Materials CHEMISTRY

Observations of defects in the layered ternary nitride, $CrWN_2$, using transmission electron microscopy

Gunnar Svensson*[a] and K. Scott Weil[b]

[a]*Department of Structural Chemistry, Stockholm University, S-10691 Stockholm, Sweden*
[b]*Department of Materials Science and Engineering, Carnegie Mellon University, Pittsburgh, PA 15213, USA*

Received 12th February 1999, Accepted 16th July 1999

Investigation of the local structure of $CrWN_2$ by electron diffraction, medium resolution electron microscopy, and image simulation verify that this nitride possesses the same rhombohedral-based structure and $AA'BB'CC'AA'BB'CC'\cdots$ layered stacking sequence as found for $LiMoN_2$. Two distinctive types of defects were observed in this compound, including twinning and intergrowth defects, which probably arise as an inherent consequence of this crystal structure type. An analysis and a description of the relationship between the crystal structure and common defects in $CrWN_2$ are discussed.

Introduction

Inorganic compounds which possess layered crystal structures often exhibit a rich array of chemical and physical properties, including low-dimensional magnetism, charge density wave phenomena, and superconductivity.[1] What is particularly intriguing about these compounds is the potential to dramatically alter their anisotropic properties through modest modifications in composition and crystal structure, as was recently observed in the electrical behavior of the layered nitrochloride Li_xZrNCl.[2] Ever since the discovery of the first layered ternary nitride phase, $NaTaN_2$, by Jacobs and von Pinkowski,[3] there has been heightened interest in exploring other layered nitride compounds and structural motifs. With respect to the more well known oxide and sulfide analogues, the expectations are that the layered ternary and higher order nitrides will display novel crystal structures, unusual cation–anion bonding arrangements, and a diverse collection of magnetic, optical, and electrical properties.[4]

Unfortunately, the unique chemistry of nitrogen presents a number of challenges when it comes to the preparation of ternary nitrides. The diffusion rate of nitrogen in many materials is typically slow, consequently high temperatures are often required to achieve reasonable solid state reaction rates. However, the high strength of the triple bond in molecular nitrogen (941 kJ mol^{-1} *vs.* 499 kJ mol^{-1} for the double bond in O_2) often gives rise to low free energies of formation and many ternary nitrides tend to be thermodynamically unstable, or only marginally stable, at elevated temperatures.[5] These problems are further exacerbated by entropic effects, which favor lower nitrogen-to-metal ratios with increasing processing temperatures. Thus, the optimal synthetic conditions of ternary nitrides are often bounded by the slow diffusion rate of nitrogen at low temperatures and by the inherent instability of these compounds at high temperatures. The difficulties in synthesis are particularly apparent with the layered ternary transition metal–transition metal nitrides; only a handful of these compounds are known. As a consequence, there is a general dearth of information with respect to the crystal chemistries and physical properties of these materials. In addition, there have been difficulties in characterizing the crystal structures of these compounds, some of which stem from the fact that most of the new nitrides have thus far been prepared only in powder form, therefore unequivocal single crystal data is not available. Of the eight known layered transition metal–transition metal nitrides reported in the literature, the proposed crystal structure models of four of these have later been questioned or amended.[6–12]

In light of the recent synthetic and characterization problems, it is apparent that in order to completely understand the structures of the layered ternary nitrides, not only is a global description of the crystal structure and bonding arrangement in the compound necessary, but so too is an account of the local structure that arises from defects and local compositional fluctuations. The local structure of crystalline materials is often best examined by transmission electron microscopy (TEM). In fact, in the past two decades, TEM has played an increasingly important role in the structural characterization of a number of solid state materials, particularly transition metal oxides, elucidating details that are often not revealed by ordinary X-ray or neutron diffraction crystallographic studies.

In an earlier report we discussed the synthesis and structural determination of $CrWN_2$ by means of Rietveld refinement using X-ray powder diffraction data. $CrWN_2$ was found to have a layered structure including layers of WN_6 trigonal prisms and CrN_6 octahedra stacked in a cubic close packed manner.[13] In this article, we report the results of our electron diffraction, medium resolution electron microscopy and image simulation studies of $CrWN_2$. The objectives of this study were two-fold: (i) to test the validity of the structural model of $CrWN_2$[13] and (ii) to catalogue and examine structural defects occurring in this particular structural type of layered nitride compound. This investigation of the defect structure of $CrWN_2$ represents one of the first transmission electron microscopy (TEM) studies on a compound from the layered nitride family.

Experimental

Nitride synthesis

Chromium tungsten dinitride, $CrWN_2$, powder was prepared by the ammonolysis of a complexed precursor, employing an approach similar to that previously reported for the preparation of other ternary transition metal nitride powders.[14] Essentially, chromium(III) chloride hexahydrate (99.995%, Aldrich) and tungsten hexachloride (99.9+%, Aldrich) were dissolved in equimolar amounts in anhydrous acetonitrile (99.8%, Aldrich). The two metal species were then simulta-

neously complexed with the bidentate chelate 1,2-diaminoethane (99%, Sigma), forming a dark green viscous liquid which settled out from the acetonitrile phase. Evaporation of the acetonitrile yielded a dark green waxy solid, which was further dried under vacuum at 90 °C for 6 h. This waxy solid was used as the precursor for $CrWN_2$. It was found that the ternary nitride could be prepared in phase-pure form with a high degree of crystallinity by heating the precursor in flowing ammonia (*ca.* 130 ml min^{-1}) at a rate of 3 °C min^{-1} to 750 °C and holding the furnace at this temperature for 20 h. The furnace was then turned off and the sample was allowed to cool inside the furnace.

Methods of characterization

The as-ammonolyzed powders were crushed in an agate mortar and mixed with butan-l-ol to form a slurry, then ultrasonicated for approximately 10 min to break up any agglomerates. In general, the ground powders were first examined by scanning electron microscopy (SEM) and energy dispersive X-ray spectroscopy (EDS) to observe the size and morphology of the nitride powder particles and to estimate the ratio of the metal constituents. A DX-4 EDS analyzer connected to an AMRAY 1810 scanning electron microscope operating at 20 kV was used to conduct the spectroscopic analyses. ZAF correction factors for chromium and tungsten in the EDS measurements were made using appropriate standards. The samples were mounted by placing a small amount of the ground powder onto a double-sided carbon tape affixed to a carbon SEM sample stub and blowing excess powder off the stub with a duster. In order to achieve a good statistical representation of the sample's metal composition, typically 10 to 20 powder particles were chosen for analysis in a given EDS measurement.

Once the ratio of chromium to tungsten in the powder had been estimated by EDS, quantitative chemical analyses were performed by Galbraith Laboratories (Knoxville, TN). Inductively coupled plasma optical emission spectroscopy was used to determine the concentration of the metal species; combustion analyses were employed to evaluate the nitrogen, carbon, and oxygen contents following the American Society for Testing and Materials standard ASTM D5373,[15] while coulometric titration was used to analyze for particularly low concentrations of these species; ion chromatography and capillary electrophoresis techniques were used to determine the chlorine levels.

X-Ray diffraction (XRD) data were collected with a Guinier–Hägg focusing camera using Cu-Kα_1 radiation and silicon as an internal standard. The X-ray films were evaluated using the SCANPI film scanner system.[16] Peaks found in the resulting XRD patterns were indexed using the DICVOL[17] indexing program and cell parameters calculated by DICVOL were further refined using the PIRUM[18] cell refinement program. Additionally, the X-ray data set was refined using the Rietveld refinement program FULLPROF,[19] in which peak shapes were represented by a modified pseudo-Voigt function[20] and atomic thermal displacements were assumed to be isotropic.

For the TEM studies, a small amount of the ground nitride sample was re-ground in butan-l-ol. The resulting dispersion was ultra-sonicated for 3 min, then allowed to settle for at least 2 min. A drop of the supernatant liquid was placed onto a holey carbon film supported by a copper grid and the butanol was allowed to evaporate. Conventional electron diffraction studies and microanalysis of single-crystallite fragments were performed using a JEOL JEM 2000 FX electron microscope operating at 200 kV (with a $+45°$ side-entry double-tilt holder). The microscope was equipped with a LINK QX200 EDS in the high angle (70°) position. The lattice image studies were conducted in a JEOL JEM 3010 microscope with a top-entry double-tilt goniometer (1.7 Å point-to-point resolution) operating at 300 kV. Simulated electron micrographs were prepared using the program suite MacTempas.[21]

Results and discussion

Phase analysis and structural model

As seen in the SEM micrographs in Fig. 1(a), despite grinding and sonication, the ammonolyzed chromium–tungsten powder still displays some agglomeration, with an agglomerate size in the order of 1–10 μm. At higher magnifications, shown in Fig. 1(b), it is apparent that the agglomerates are composed of platelet-shaped microcrystals. The microcrystals were typically found to be 40–80 nm in diameter, with thicknesses between approximately 8 and 12 nm. This morphology was taken to be an indication of the underlying layered crystal structure of the compound, which was later confirmed by X-ray and electron diffraction analyses.

Semi-quantitative analysis of several powder samples using EDAX consistently gave Cr/W ratios of near unity, in good agreement with the expected value of 1.0. These results were confirmed on a more local scale by EDS on the JEM 2000 FX instrument. Similarly, results from the chemical analyses, shown in Table 1, verify the stoichiometry of the ammonolyzed Cr–W compound as $CrWN_2$. The slight nitrogen deficiencies observed in these samples are similar to those reported previously for the same compound.[13] It should be noted that all of the impurities (O, C, Cl) that one might expect to be found in the product, derived from the chelation preparation technique described above, are all low in concentration (below 1000 ppm).

Although the lines observed in the XRD film for this compound were somewhat diffuse, the *d*-spacing values at FWHM of the corresponding peaks observed in the SCANPI-interpreted diffraction pattern were found to match those reported for $CrWN_2$.[13] No extraneous lines were observed. Based on the indexing results from DICVOL and PIRUM, the observed peaks over the 0–90° 2θ range fit the $CrWN_2$ indexing scheme with a de Wolff[22] figure of merit of $M_{18}=238$. Least squares refinement of the lattice parameters, using a hexagonal notation, yielded values of $a=2.845(8)$ Å and $c=15.617(2)$ Å. Results from the Rietveld refinement displayed excellent agreement with those found in the previous study, yielding lattice and atomic parameters within 1–2% of the published data. The refinement converged with the following residuals: $R_{wp}=0.054$, $R_p=0.043$, $R_I=0.0203$, $D_{wd}=1.08$, and $\chi^2=0.97$. Based on the verification provided by this analysis, the data from ref. 13 were employed in the structural models for the TEM studies.

Thus far, all of the known layered ternary transition metal nitrides fall into two structural categories, either hexagonal or rhombohedral.[5–12] The structural variations between these two different forms, as well as between the variants within each category, due to stacking of the constituent layers are relatively subtle. According to the reported structural model for $CrWN_2$, the atoms in this nitride were found to be distributed over the following Wyckoff positions in the trigonal *R*3 (146) space group, hexagonal axes: 1 Cr in 3(a) at (0, 0, 0.8251(7)), 1 W in 3(a) at (0, 0, 0), 1 N in 3(a) at (0, 0, 0.2629(6)), and 1 N in 3(a) at (0, 0, 0.4068(5)). Thus, ideally, $CrWN_2$ consists of alternating sheets of nitrogen atoms according to the packing sequence a–a–b–b–c–c. The tungsten atoms are found with trigonal prismatic coordination in the a–a, b–b and c–c layers of nitrogen atoms and the chromium atoms are sandwiched within octahedral interstices formed between the adjacent close packed nitrogen layers; a–b, b–c, c–a *etc*. These polyhedral arrangements are represented in Fig. 2(a). The alternating layers of edge-sharing WN_6 trigonal prisms and edge-sharing CrN_6 octahedra are stacked in an AA′BB′CC′ manner along

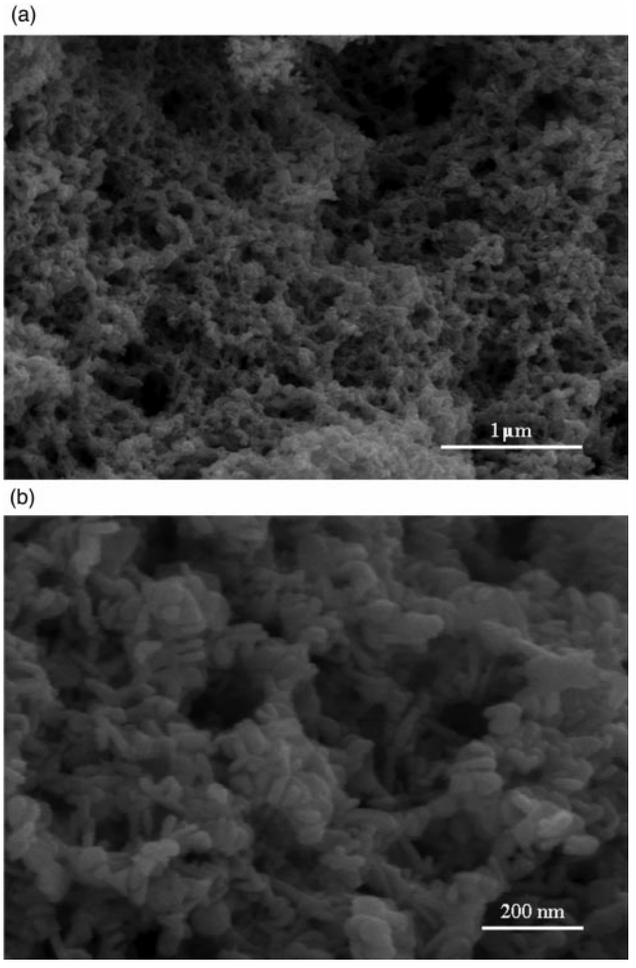

Fig. 1 SEM micrographs showing the morphology of the nitride powder particles obtained after heat treating the precursors at 750 °C for 20 h in ammonia: (a) at 10 000 × magnification and (b) at 125 000 × magnification.

the *c*-axis, as shown in Fig. 2(b), thus defining a trigonal structure as opposed to a hexagonal structure, where A, B, and C are the WN_6 layers and A′, B′, and C′ are the CrN_6 layers.

A second means of visualizing the layered arrangement of $CrWN_2$, which is particularly instructive when interpreting layering defects in this material, is to recognize that the nitrogen layers on either side of any given tungsten layer are stacked in coincident pairs, with one adjacent nitrogen layer positioned directly over the other. As shown in Fig. 2(b), these paired nitrogen layers are stacked in $CrWN_2$ in an a–a–b–b–c–c–a⋯ arrangement in a manner similar to that seen in FCC stacking. From this perspective, the chromium layers 'dictate' the forward $+1/3,+1/3$ shift of N–W–N slabs in the *x*,*y* plane as they are stacked along the *c*-axis. As a result, an adjacent WN_6 trigonal prism layer can act as a potential twinning plane for a stacking shift in the negative direction, *i.e.* $-1/3,-1/3$.

Table 1 Chemical analysis of the nitrided Cr–W product

Concentration/ atom% or ppm	Sample 1	Sample 2	Theoretical
%Cr	25.86	25.69	25.00
%W	25.52	25.41	25.00
%N	48.27	48.46	50.00
ppm C	875	830	0
ppm O	222	374	0
ppm Cl	844	763	0

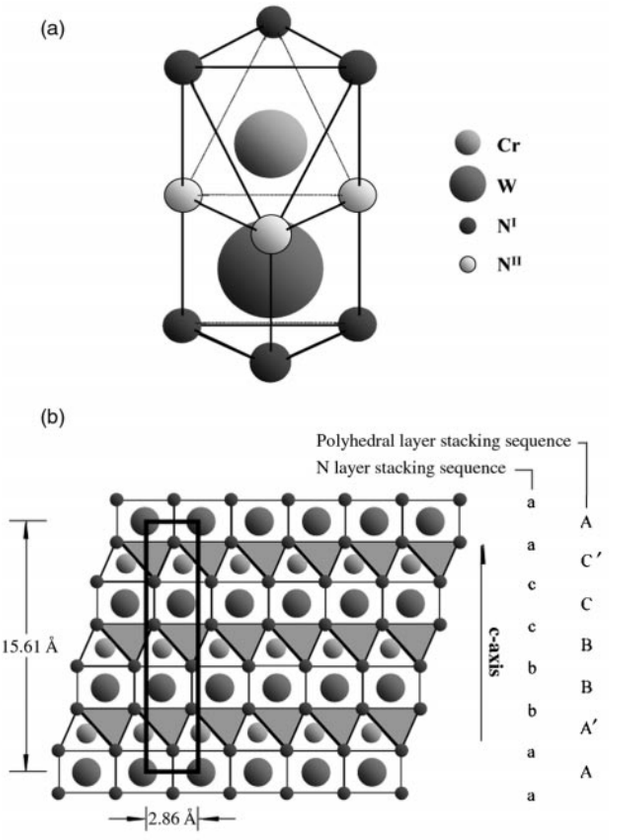

Fig. 2 Proposed structure for $CrWN_2$ displaying: (a) a polyhedral model of the trigonal prismatic coordination of nitrogen around tungsten and of the octahedral nitrogen coordination around chromium, and (b) the stacking sequence of the WN_6 trigonal prism layers and the CrN_6 octahedral layers, or alternatively the nitrogen layers, in $CrWN_2$. The unit cell of $CrWN_2$ is outlined by the heavy black lines.

Structural defects: stacking faults (twinning)

Most of the crystallites studied with the transmission electron microscope were oriented in the a–b plane. This is not surprising considering the two dimensional nature of the structure. No superstructure reflections were observed in the electron diffraction patterns taken along $<001>$. The electron diffraction (ED) patterns recorded along the $<100>$ directions exhibited systematic absences, $-h+k+l=3n$, in agree-

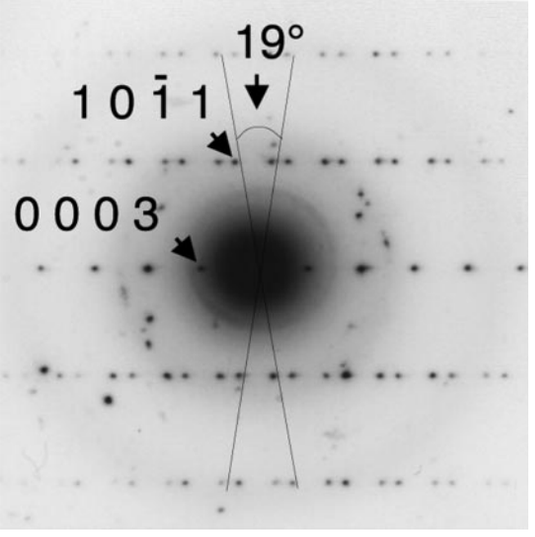

Fig. 3 Electron diffraction pattern of a twinned $CrWN_2$ crystallite taken along [010].

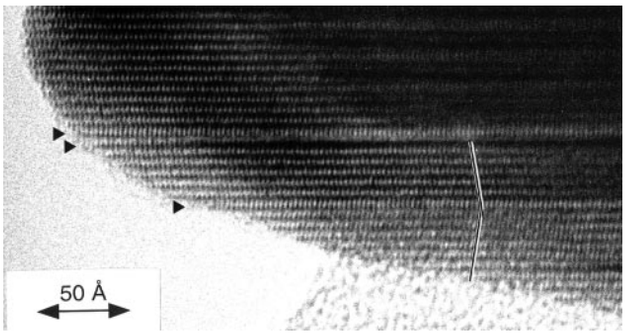

Fig. 4 Electron micrograph of a crystallite with twinning recorded close to the Scherzer focus (−412 Å). The arrows on the left denote the twinning planes in the structure. The lattice fringes are tilted by *ca.* 19° across the twin boundary, as shown by the black-on-white lines.

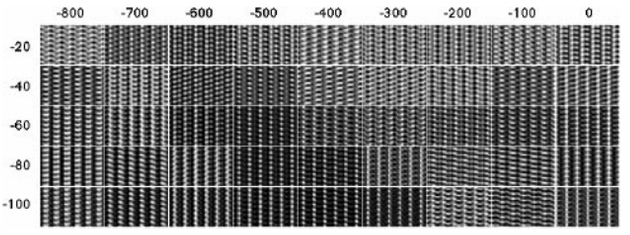

Fig. 5 Simulated electron micrographs (defocus, horizontal; thickness, vertical) of $CrWN_2$.

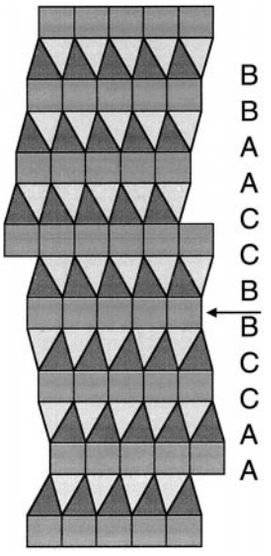

Fig. 6 A structure model showing a twin defect. The packing sequence of the nitrogen ions is given.

Fig. 7 Electron micrograph showing a group of intergrown crystallites. Regions marked as A, B, and C, and as D, denoted by the arrows in the figure, are magnified in Fig. 8 and 10, respectively.

ment with space group $R3$ (hexagonal setting). The hexagonal setting will be used below. In general, the ED patterns and simulated electron micrographs observed in this investigation confirm the Rietveld refinement results in this study, and thus those of the previously reported structural model for $CrWN_2$. However, the ED patterns frequently revealed the existence of twinning in the {001} planes, as seen in Fig. 3.

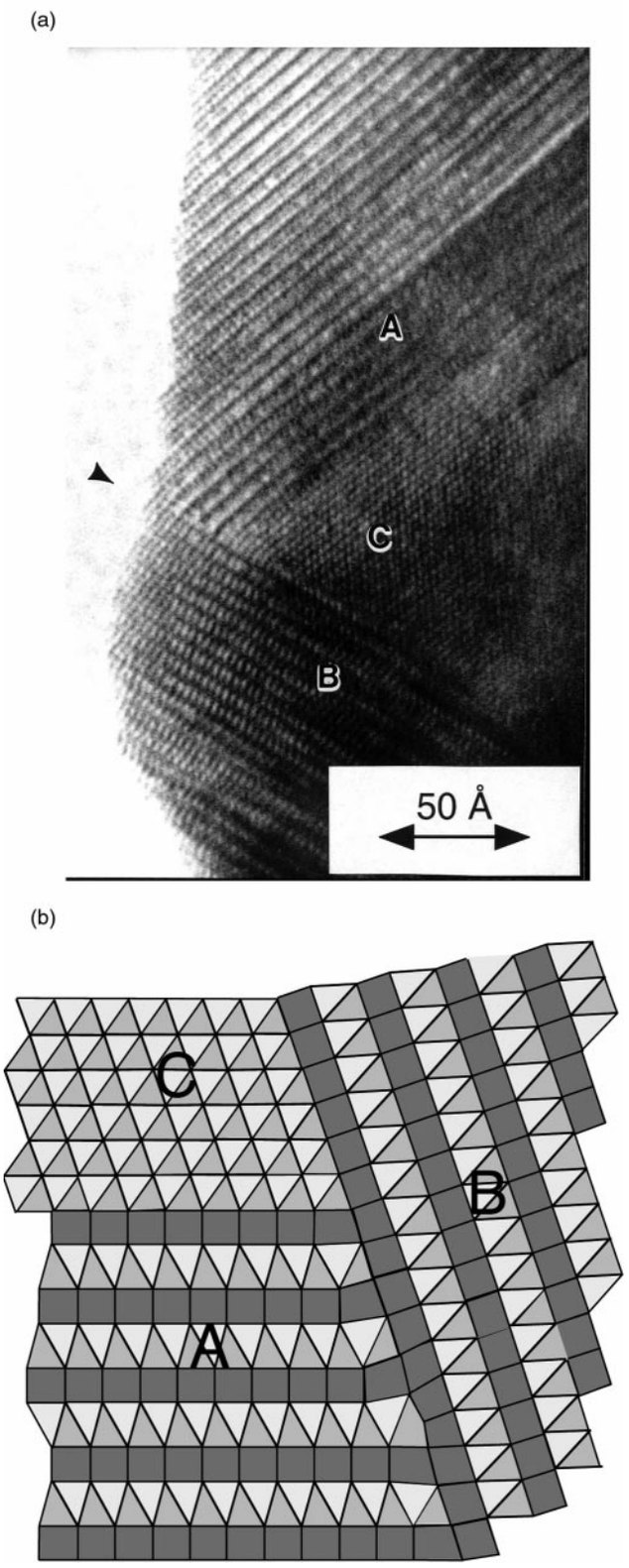

Fig. 8 (a) A magnification of the area in Fig. 7 marked as A, B, C. Regions A and B consist of $CrWN_2$ intergrown along {102} and {001}, respectively. Region C appears to be composed of cubic close-packed CrN. (b) A structural interpretation of the triple junction in (a).

A TEM image which displays examples of this type of defect in $CrWN_2$ is shown in Fig. 4. A simulation of this image using the atomic coordinates previously published for $CrWN_2$ is shown in Fig. 5. A comparison between the observed image, taken close to the Scherzer focus (defocus −412 Å), and the simulated image shows good agreement for a crystal thickness of 60 Å at the crystallite's edge, marked by the lower arrow on the left-hand side of Fig. 4. At this imaging condition, the dark contrasts correspond to tungsten atoms, while the chromium atoms are seen as a pale gray contrast. The coherent boundaries of one pair of twins are marked by the double arrows in the upper left corner of the electron micrograph. The black-on-white lines on the lower right-hand side of the image highlight the tilt angle across the coherent boundary of a third twin. As described in the preceding section, the twinning is caused by mirror planes in the trigonal prismatic layers. The packing sequence of the nitrogen ions is then b–b–a–a–c–c–b–|–b–c–c–a–a as seen in the structural model shown in Fig. 6. The tilt angle between the lattice fringes in the electron micrograph is 19°, in agreement with what was observed in the ED patterns and the structural model.

Structural defects: intergrowth defects

In addition to twinning, intergrowth defects were also frequently found in the microstructure of $CrWN_2$, an example of which is displayed in Fig. 7 (the image is recorded close to the Scherzer focus). The fragment marked as A in this figure is a crystallite of $CrWN_2$ as viewed along a $<100>$ axis. Grown into this fragment and also oriented along $<100>$, but rotated counter-clockwise 72° to the layers in A is a second fragment of $CrWN_2$, marked as B. The intergrowth planes for A and B are {102} and {001}, respectively. At the triple point between the two $CrWN_2$ crystallites a different crystalline pattern is seen, marked C. A reasonable interpretation of the structure of this third region is that it consists of cubic CrN,[23] of the rock salt type, as viewed along [110]. A magnification of this area and a structural model showing how this triple junction can be accommodated into the structure without larger structural arrangements are shown in Fig. 8(a) and (b). The angle between the $CrWN_2$ units in the model is 72°, in good agreement with what was observed in the image. A reasonable agreement between the simulated images in Fig. 5, and the area marked B in the electron micrograph (defocus *ca.* −400 Å), shown in Fig. 8, is found for a crystal thickness of 60 Å. An image simulation for cubic close-packed CrN shows a good correspondence with the image at −400 Å and 60 Å, close to C in the observed image, as shown in Fig. 9.

The idea that region C is CrN is supported by the two-layer intergrowth defect at D in Fig. 7. A magnification of this defect together with an interpretation is shown in Fig. 10(a) and (b). The defect appears to consist of an extra layer of CrN_6 octahedra inserted between the layers of WN_6 trigonal prisms giving a double layer of CrN_6 octahedra. Assuming that the composition of this defect is CrN, its occurrence in $CrWN_2$ is

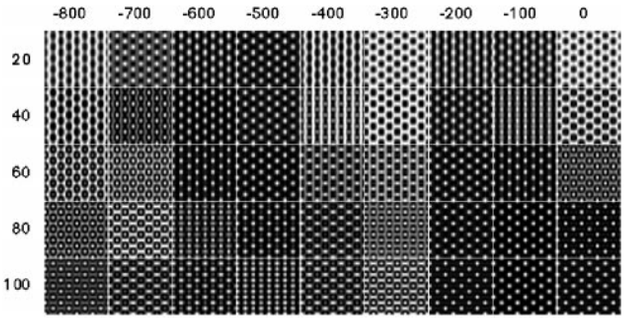

Fig. 9 Simulated electron micrographs (defocus, horizontal; thickness, vertical) of cubic CrN.

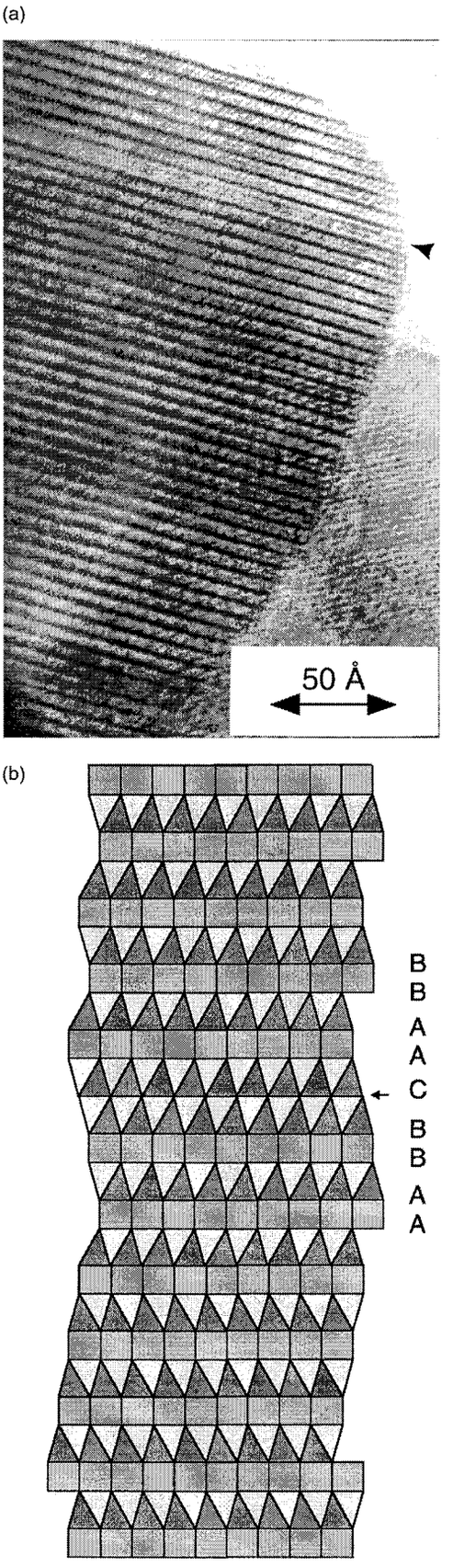

Fig. 10 (a) A magnification of area D in Fig. 7. Shown in this image is a two-layer thick intergrowth defect. As seen to the left of the arrow, an extra layer of CrN_6 octahedra appears to be inserted between the two sheets of WN_6 trigonal prisms, thus forming a double layer of octahedra. A model of the defect in (a) is displayed in (b).

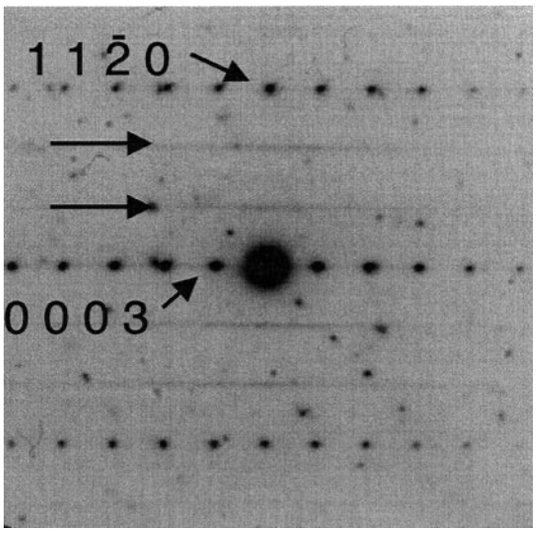

Fig. 11 An electron diffraction pattern of $CrWN_2$ along $<1\bar{1}0>$ with streaking along $\langle 001\rangle^* = \langle 0001\rangle^*$ at $1/3\langle 110\rangle^* = \langle 11\bar{2}0\rangle^*$.

interesting. It implies that the ternary nitride and CrN may have similar free energies of formation under the given heat treatment conditions. Additionally, it suggests that as the ternary nitride phase nucleates and grows during ammonolysis, the occasional formation of this double layer may act as a site for coherently templating additional layers of CrN_6, forming the more extensive intergrowth region of CrN seen in Fig. 8(a). Note, from the structural model in Fig. 8(b), that the octahedral planes of the intergrown CrN fragment can subsequently act as potential sites for the coherent nucleation and growth of $CrWN_2$. Ultimately, high spatial microanalysis will be required to determine if the area marked C is CrN.

In some of the ED patterns recorded along $\langle 1\bar{1}0\rangle$ diffuse streaks are seen parallel to the reciprocal c^* axis intersecting the reciprocal $[110]^* = \langle 11\bar{2}0\rangle^*$ axis at 1/3 and 2/3, as shown in Fig. 11. This is, typically, an indication of disordering phenomena. However, its coincidence with the observation of the CrN intergrowth defects could not be rigorously established and thus the exact origin of this streaking remains unknown.

Conclusions

The crystal structure and local microstructure of the layered ternary nitride, $CrWN_2$, have been studied by medium resolution transmission electron microscopy combined with electron diffraction and image simulation. The experimental results confirm that $CrWN_2$ is a layered compound crystallizing in the *R*3 space group. The layering sequence consists of alternating sheets of edge-sharing CrN_6 octahedra and edge-sharing WN_6 trigonal prisms stacked in an AA′BB′CC′⋯ FCC-like fashion along the *c*-axis. Shifting of the chromium layers in this sequence was found to occur quite frequently, leading to the formation of coherent twins in the $CrWN_2$ microstructure. Evidence of coherent intergrowth defects, of variable thickness, was also observed. Based on the structural models of $CrWN_2$ and of CrN in the rock salt configuration, image simulations of the intergrowth regions suggest that they are likely composed of chromium nitride.

Acknowledgements

We gratefully acknowledge Dr Jekabs Grins for his help in refining the XRD data and for his support of this work. We also wish to thank the Swedish Natural Science Research Council for financial support of this study. In addition, K.S.W. would like to thank the Electrochemical Society for the F. M. Becket Memorial Fellowship that made it possible for him to study at Stockholm University.

References

1 P. A. Salvador, T. O. Mason, M. E. Hagerman and K. Poeppelmeier, in *Chemistry of Advanced Materials*, ed. L. V. Interrante and M. J. Hampden-Smith, John Wiley & Sons, New York, 1998, ch. 10.
2 S. Yamanaka, K. Hotehama and H. Kawaji, *Nature*, 1998, **392**, 580.
3 H. Jacobs and E. von Pinkowski, *J. Less-Common Met.*, 1989, **146**, 147.
4 H.-C. zur Loye, J. D. Houmes and D. S. Bem, in *The Chemistry of Transition Metal Carbides and Nitrides*, ed. S. T. Oyama, Chapman & Hall, London, 1993, ch. 7.
5 S. H. Elder, F. J. DiSalvo, L. Topor and A. Navrotsky, *Chem. Mater.*, 1993, **5**, 1545.
6 J. D. Houmes, D. S. Bem and H-C zur Loye, in *Mater. Res. Soc. Symp. Proc.: Covalent Ceramics II—Non-Oxides*, ed. A. R. Barron, G. S. Fischman, M. A. Fury and A. F. Hepp, Materials Research Society, Boston, MA, 1993, vol. 327, p. 165.
7 D. S. Bem and H-C zur Loye, *J. Solid State Chem.*, 1993, **104**, 467.
8 D. S. Bem, C. M. Lampe-Önnerud, H. P. Olsen and H.-C. zur Loye, *Inorg. Chem.*, 1996, **35**, 581.
9 D. S. Bem, J. D. Houmes and H-C zur Loye, in *Mater. Sci. Forum: Soft Chemistry Routes to New Materials—Chimie Douce*, ed. J. Rouxel, M. Tournoux and R. Brec, Trans Tech Publications, Switzerland, 1993, vol. 152–153, p. 183.
10 J. Grins, P-O. Käll and G. Svensson, *J. Mater. Chem.*, 1995, **5**, 571.
11 P. S. Herle, N. Y. Vasanthacharya, M. S. Hegde and J. Gopalakrishnan, *J. Alloys Compd.*, 1995, **217**, 22.
12 K. S. Weil and P. N. Kumta, *Acta Crystallogr., Sect. C*, submitted.
13 K. S. Weil and P. N. Kumta, *J. Solid State Chem.*, 1997, **128**, 185.
14 K. S. Weil and P. N. Kumta, *J. Solid State Chem.*, 1997, **134**, 302.
15 ASTM D5373-93(1997), Standard Test Methods for Instrumental Determination of Carbon, Hydrogen, and Nitrogen in Laboratory Samples of Coal and Coke.
16 K-E. Johansson, T. Palm and P-E. Werner, *J. Phys. E*, 1980, **13**, 1289.
17 A. Boultif and D. Louer, *J. Appl. Crystallogr.*, 1991, **24**, 987.
18 P.-E. Werner, *Ark. Kemi*, 1969, **31**, 513.
19 J. Rodriguez-Carvajal, M. T. Fernandez-Diaz and J. L. Martinez, *J. Phys.: Condens. Matter*, 1991, **3**, 3215.
20 P. Thompson, D. E. Cox and J. B. Hastings, *J. Appl. Crystallogr.*, 1987, **20**, 79.
21 R. Kilaas, MacTempas: Program For Simulating High Resolution TEM Images and Diffraction Patterns, Total Resolution, Berkeley, CA, 1994.
22 P. M. deWolff, *J. Appl. Crystallogr.*, 1968, **1**, 108.
23 R. Blix, *Z. Phys. Chem., Abt. B*, 1929, **3**, 229.

Paper 9/01188I